Proceedings of the Combustion Institute 42 (2026) 106657

Contents lists available at ScienceDirect

Proceedings of the Combustion Institute

journal homepage: www.elsevier.com/locate/proci

Synergistic use of plasma and air staging for emission control in NH_3–air flames

B Aravind *, Ziyu Wang, Syed Mashruk, Agustin Valera-Medina

College of Physical Sciences and Engineering, Cardiff University, Wales, CF24 3AA, UK

ARTICLE INFO

Keywords:
Net zero
Emission
Hydrogen
Power generation
Plasma assisted combustion

ABSTRACT

In this study, a detailed experimental investigation on the effect of gliding arc plasma on the emission characteristics of air staged (AS) ammonia (NH_3) flames is conducted for the first time. Four AS configurations, AS-OI-L100, AS-OI-L200, AS-TI-L100, and AS-TI-L200 employing orthogonal (OI) and tangential (TI) secondary air injections at two axial locations (100 mm and 200 mm) were examined. For no-plasma cases, the results show that AS significantly reduces NO emissions compared to the no-staged configuration, with AS-OI-L200 achieving 73–77 % NO reduction while maintaining minimal NH_3 slip (<5 ppm). Tangential injection further enhanced NO reduction (up to 85 %) but increased NH_3 slip, whereas a shorter staging distance (L100) led to reduced performance due to limited mixing. Plasma activation markedly improved flame stability and radical formation, providing an additional 36–38 % NO reduction relative to no-plasma cases. Moreover, the combined plasma–AS operation achieved up to 96 % NO reduction under lean conditions, although excessive NH_3 slip was observed in some tangential configurations. Overall, the AS-OI-L200 configuration exhibited the most balanced performance, delivering high NO reduction alongside low NH_3 and N_2O emissions. Numerical analysis further reveals that plasma activation increases NH_2 concentrations, shifting NO formation from the conventional Fuel-N pathway toward an N-activated oxidation route. When combined with air staging, reduced local O_2 availability and enhanced NO consumption via $N + NO = O + N_2$ lead to net suppression of NO formation. These findings demonstrate that careful control of secondary air injection orientation and staging location, in combination with plasma activation, provides an effective strategy for achieving stable, low-emission NH_3 combustion, thereby advancing the practical use of ammonia as a carbon-free fuel.

Novelty and significance statement: This study presents the first experimental demonstration of a dual-control strategy that integrates plasma-assisted combustion in the primary zone with air staging in the secondary zone for active emission control in NH_3–air flames. The proposed approach effectively achieves simultaneous mitigation of both ammonia slip and NO emissions, demonstrating approximately 80 % reduction in NO while maintaining minimal NH_3 slip (<5 ppm) compared to no-staged conditions. This advancement not only enhances flame stability and combustion efficiency but also paves the way for clean, controllable, and scalable ammonia-based combustion technologies, accelerating the transition toward carbon-neutral energy production.

1. Introduction

Over the past decade, ammonia (NH_3) has attracted significant attention from the energy sector as a viable carbon-neutral fuel owing to its high hydrogen density and good transport properties [1,2]. Despite these advantages, NH_3 combustion faces major challenges, including poor ignition characteristics and high nitrogen oxide (NO_x) emissions, which hinder its direct application in power and propulsion systems [3]. To overcome these limitations, several strategies have been explored, such as cofiring with reactive fuels such as methane (CH_4) and hydrogen (H_2) [4–10], staged combustion [11–19], humidification [20], fuel stratification [21], and plasma-assisted combustion [22,23] etc.

Among these techniques, air-staged combustion has been widely explored in recent years as an effective technique to reduce the emissions in NH_3 flames [11–19]. In the air staging, the primary zone typically operates under fuel-rich conditions, where NH_3 partially decomposes to form intermediate species such as H_2 and NH_x radicals. Additional air is then introduced in the secondary zone to complete the

* Corresponding author.
E-mail address: balakrishnana4@cardiff.ac.uk (B. Aravind).

https://doi.org/10.1016/j.proci.2026.106657
Received 15 March 2026; Accepted 5 June 2026
Available online 9 October 2026
1540-7489/© 2026 Published by Elsevier Inc. on behalf of The Combustion Institute.

oxidation process. This staged oxidation strategy modifies the nitrogen conversion pathways and reduces peak temperatures, thereby suppressing NO formation [12,13].

Somarathne et al. [12] performed large-eddy simulations of NH_3-CH_4-air premixed swirling combustion and showed that air staging with a primary-zone equivalence ratio of approximately 1.2 significantly reduces NO emissions to around 100 ppmvd. Liu et al. [14] modelled the secondary air injection and found that staging enhances the oxidation near the combustor outlet while promoting reactions such as $NO + O + M = NO_2 + M$ and $NO + OH = NO_2 + H$, which contribute to lowering NO concentrations. Okafor et al. [15] experimentally demonstrated that the secondary air injection in the NH_3—CH_4-air gas turbine swirl combustor can nearly eliminate NH_3 slip while maintaining relatively low NO_x emissions. However, fuel-rich primary zones may also lead to incomplete fuel conversion, NH_3 slip, and combustion instabilities, which restrict the operational stability range of the combustor [16–19]. For instance, Pugh et al. [16,17] also highlighted the trade-off between minimising unreacted NH_3 and controlling NO_x formation. Recently, Avila Jimenez et al. [18] demonstrated that secondary air injection can significantly reduce NO emissions by roughly ten times compared to single-stage lean combustion, and it also helps reduce N_2O emissions. However, they also observed low-frequency flame instabilities originating in the primary zone [19]. This underscores the need to combine multiple emission-control strategies to further lower the emission characteristics, an approach that has not yet been explored. This is the key focus of the present study.

Plasma-assisted NH_3 combustion (PAAC) using non-equilibrium plasmas has recently emerged as another promising technique for improving flame stability and influencing emission characteristics [22–24]. In PAAC systems, non-equilibrium plasmas generate energetic electrons that produce reactive radicals such as O, H, and OH, which can alter the chemical reaction time scales and enhance ignition processes [25]. The effect of various non-equilibrium plasmas including nanosecond repetitively pulsed (NRP) discharges, dielectric barrier discharge (DBD), and gliding arc plasma (GAP), on the combustion characteristics of NH_3-air have been investigated [26–40]. Choe et al. [26] were the first to demonstrate that NRP discharges extend lean blowout (LBO) limits while reducing NO_x emissions in NH_3-air flames. Later, Kim et al. [27] reported that DBD plasma enhances NH_2* radical formation, leading to a strong reduction in NO_x emissions. In the last five years, significant research has investigated the impact of gliding arc plasma (GAP) on NH_3-air and NH_3—CH_4 mixtures [28–34]. For example, Tang et al. [33] employed GAP to stabilise NH_3 swirling flames under ultra-lean operating conditions, achieving low NO emissions. Using the same combustor configuration, Sun et al. [34] later investigated NH_3—CH_4 fuel blends and reported improved flame stability along with reduced emissions. Ju et al. [36] investigated NH_3-air premixed swirling flames with rotating GAP and analysed the spatial distribution of radicals using OH-PLIF diagnostics. Furthermore, recent review articles on the PAAC have emphasised the need for further research to understand the interaction between plasma-generated radicals and NH_3 combustion chemistry, particularly with respect to emission formation mechanisms [22,23]. However, despite these advances in the PAAC, most studies have primarily focused on improving flame stability and extending flammability limits, with relatively limited attention given to NO_x mitigation mechanisms. In particular, the production of oxygen-containing radicals such as O and OH during plasma actuation can promote NO formation through the HNO pathway, which contributes to a large fraction of NO_x formation in NH_3 flames [8].

In our previous work [28,30], a selective PAAC strategy was developed to address this limitation. In this approach, plasma was applied only to the NH_3 fuel stream prior to mixing with air, which enhanced NH_2 radical formation while limiting plasma-air interaction and reducing excessive OH production. This configuration promoted De-NO_x pathways and resulted in significant reductions in NO and NO_2 emissions. Plasma actuation also extended lean and rich blowout limits by approximately 15–20 % and 30–35 %, respectively. A similar strategy was successfully tested in a swirl burner by Lin et al. [32,35]. However, under near-stoichiometric conditions, incomplete fuel conversion led to noticeable NH_3 slip, which limits the practical application of this approach [30].

To address this limitation, the present study for the first time proposes a dual-control strategy that combines plasma-assisted combustion in the primary zone with air staging in the secondary zone. A systematic parametric investigation is performed to evaluate the effects of air-staging configuration and injection location on emission characteristics of plasma assisted NH_3 flames. In addition, kinetic modelling is conducted to elucidate the mechanisms governing NO_x formation and reduction in PAAC.

2. Experimental setup and methodology

The experiments were conducted using a novel plasma assisted dual-swirl combustor as shown in Fig. 1. The overall configuration and the dimensions of the experimental rig was identical to that described in the authors' previous studies [28,30]. Combustion air supplied through the annular gap between the nozzle and the fuel lance, providing a premixing length of 2.5 mm. A rotating gliding arc plasma was generated inside the fuel lance using a conical central electrode made up of tungsten-steel alloy positioned coaxially with the lance. The electrode also acted as a bluff body and provides a minimum annular gap of 2 mm to initiate the gliding arc discharge. The electrode tip-to-dump plane distance of 3 mm, promoting arc rotation along the swirling NH_3 jet. This ensures This configuration ensured that the plasma interacted primarily with the NH_3 stream, thereby limiting NO formation through the HNO pathway [35]. The plasma excitation frequency was maintained at 13 kHz, and the input voltage was adjusted to maintain a constant plasma-to-flame power ratio of approximately 1.5 % with an approximate average plasma power of 100 W. The plasma power was kept constant to enable a fair comparison of the plasma effects on the combustion characteristics. The typical temporal evolution of electrical characteristics including voltage, current and the power is also illustrated in the Fig. 1.

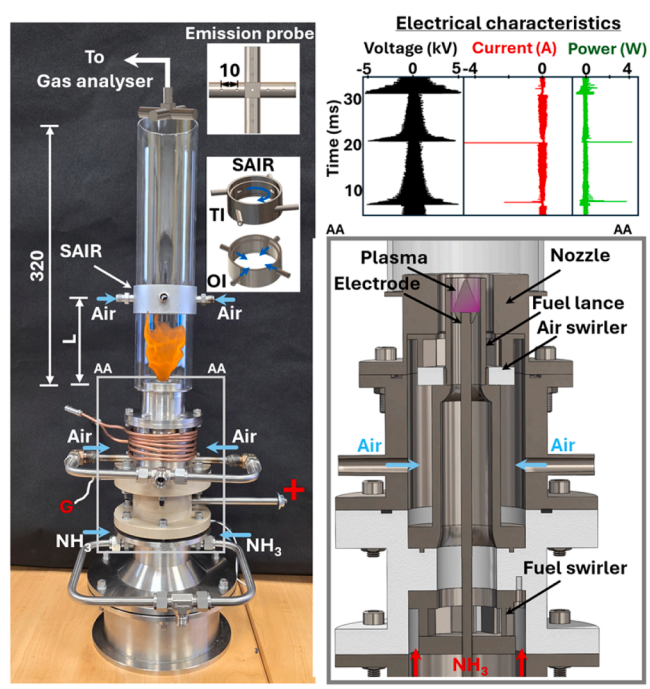

Fig. 1. Schematic of the experimental setup with typical electrical characteristics.

For the no-staging (NS) configuration, a 320 mm long quartz tube with an internal diameter of 68 mm was used to confine the flame. On the other hand, for the air staging (AS) configuration, a secondary air injection ring (SAIR) of 20 mm length was installed axially between two quartz tubes of 200 mm and 100 mm lengths as shown in Fig. 1. Two SAIR axial positions of 100 mm and 200 mm downstream of the dump plane were investigated for both orthogonal (OI) and tangential (TI) air injection modes. For OI, secondary air entered through four nozzles of 6 mm diameter positioned perpendicular to the main flow, while for TI, tangential nozzles with the same dimensions were used to generate a clockwise secondary air swirl. The details of the AS conditions are summarised in Table 1.

The diagnostic systems for flame imaging, electrical and emission measurement are the same as those used in the authors' previous study, and their details are omitted in the Fig. 1 for brevity [30]. The voltage and current waveforms were measured using a Tektronix P6015 High Voltage Probe and a Cybertek HCP 8030 Current Probe, respectively. The signals were acquired using a Tektronix MSO64B Oscilloscope for time-resolved electrical diagnostics. Chemiluminescence imaging was performed using three synchronized LaVision CCD Camera System operating at 10 Hz. For each operating condition, 200 image frames were acquired using LaVision DaVis v10 software and subsequently processed through time-averaging, background subtraction, and Abel inversion to reconstruct axisymmetric emission fields. Spectrally resolved chemiluminescence from OH*, NH*, and NH_2* radicals was obtained using narrow bandpass optical filters centered at 309 nm (±10 nm FWHM), 336 nm (±10 nm FWHM), and 630 nm (±10 nm FWHM), corresponding to the OH* ($A^2\Sigma^+$–$X^2\Pi$), NH* ($A^3\Pi$–$X^3\Sigma^-$), and NH_2* emission bands, respectively [41]. Exhaust gas species, including NO, N_2O, NO_2, NH_3, O_2, and H_2O, were measured using an Emerson CT5100 Gas Analyser operating at a sampling frequency of 1 Hz, with a repeatability of ±1 % and linearity of 0.999. Gas samples were extracted using a cross-probe fitted with ten 2 mm holes, each spaced at 10 mm intervals, and positioned 10 mm above the quartz tube exit to ensure representative sampling of the exhaust flow as shown in Fig. 1. To avoid condensation of water vapor and ammonia in the sampling line, the transfer line was maintained at 463 K throughout the measurements. For each test condition, 120 samples were recorded, averaged, and finally normalized to a dry basis with 15 % O_2 correction [8].

2.1. Numerical methodology

To understand the effect AS in the plasma assisted NH_3 flames, numerical simulations were performed using an integrated ZDPlaskin–Chemkin model by Wang et al. [29]. This approach is widely used in plasma-assisted NH_3 combustion studies [36,38] and follows procedures similar to those of Crispim et al. [42] and Dong et al. [43]. The plasma-assisted combustion mechanism developed by Wang et al. [29] integrating the plasma reactions from Mao et al. [36] with the NH_3 combustion mechanism of Alnasif et al. [44], is used in the present study. The reaction mechanism consists of 78 species and 238 reactions. Simulations incorporate current and voltage characteristics of the arc as initial electron field (E/N) and electron density inputs to capture kinetic changes induced by the gliding arc. For modelling the AS, combination of a perfectly stirred reactor (PSR) and a plug flow reactor (PFR) is employed at each stage, with parameters defined based on the actual burner geometry. The PFRs have lengths of 100 mm (primary stage) and 200 mm (secondary stage), both with a diameter of 68 mm. The residence time in each reactor is calculated self-consistently from the corresponding flow rate and reactor volume. The inlet conditions are specified as a temperature of 300 K and a pressure of 1 atm (ambient conditions). The schematic of the numerical methodology is shown in Fig. S1 of the supplementary material. Furthermore, the present numerical model has been successfully validated against experiments under different operating conditions, including NS, AS, and plasma+AS, as shown in Fig. S2 of the supplementary material.

Table 1
Details of AS conditions used in the present study.

Category	Mode	Injection	Stage location
NS	No-staging	-	-
AS-TI-L200	Staging	Tangential	200
AS-TI-L100	Staging	Tangential	100
AS-OI-L200	Staging	Orthogonal	200
AS-OI-L100	Staging	Orthogonal	100

3. Results and discussion

3.1. Effect of air staging on emissions

In this section, the impact of different AS configurations on the emission profiles of NO, NO_2, N_2O, and NH_3 is analysed and compared with NS conditions for various overall equivalence ratios ($\phi_{overall}$) as shown in Fig. 2. For NS cases, significant NH_3 slip is observed on the rich side ($\phi_{overall} > 1$), while NO levels remain relatively low (Fig. 2(a) and Fig. 2(d)). Furthermore, author's previous study showed that plasma effects can shift this NH_3 slip toward leaner conditions, occurring even at $\phi_{overall} = 0.96$ [28]. Therefore, in the present study, ϕ_{pri} is fixed at 1.1, and secondary air is introduced to investigate emission profiles at $\phi_{overall} = 0.85$, 0.91, and 1.0, where $\phi_{pri} = \phi_{overall}$ for NS case. Fig. 2 reveals that secondary air injection significantly reduces NO emissions,

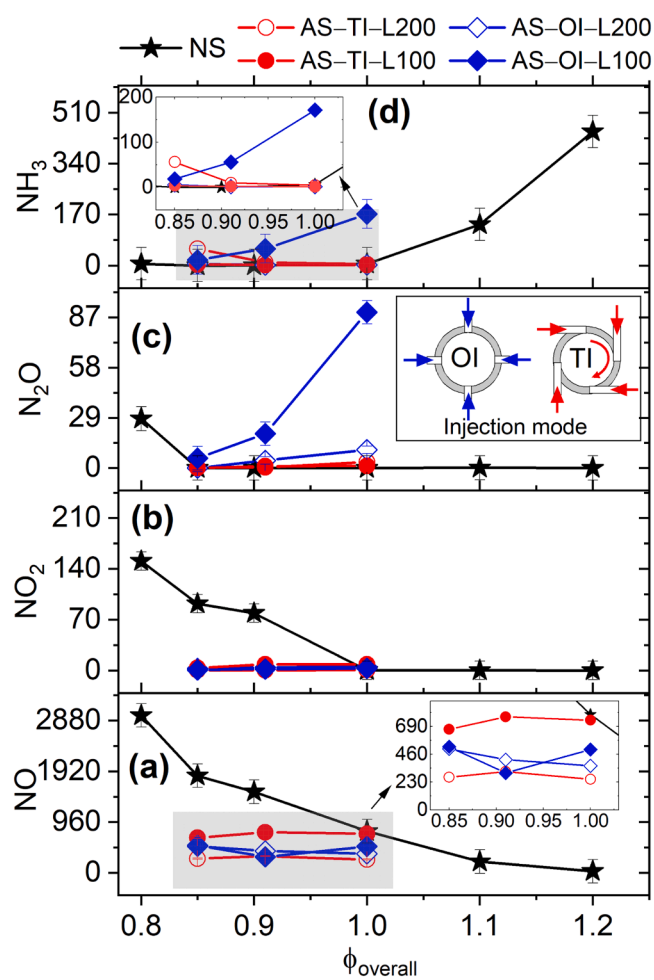

Fig. 2. Variation of (a) NO, (b) NO_2, (c) N_2O and (d) NH_3 with $\phi_{overall}$ for different AS configuration at fixed ϕ_{pri} =1.1 (All emissions are normalized to dry 15 % O_2).

particularly at leaner conditions.

The AS-TI-L200 configuration demonstrates the highest NO reduction of 83–85 % compared to NS case, while AS-OI-L200 and AS-OI-L100 achieve reductions of 73–78 % at $\phi_{overall}$=0.85 and 0.91. The AS-TI-L100 configuration, in contrast, only reduces NO by 58–65 %, likely due to insufficient penetration and poor impingement of the secondary air [11]. The NH_3 slip is achieved well below 20 ppm for AS-OI-L200, AS-TI-L100, whereas AS-TI-L200 exhibits a significant NH_3 slip of 56 ppm at $\phi_{overall}$ = 0.85, although it drops to zero at $\phi_{overall}$ = 0.94. However, the AS-OI-L100 configuration shows an increasing trend in NH_3 slip, rising from 19 ppm to 172 ppm as the $\phi_{overall}$ increases from 0.85 to 1.0. Interestingly for all the AS cases, near-zero levels of NO_2 are achieved for all the $\phi_{overall}$ as shown in Fig. 2(c). Furthermore, N_2O emission shows increasing trend with $\phi_{overall}$ for AS-OI-L100 cases while maintaining <20 ppm for all other AS cases. This increase in N_2O for AS-OI-L100 is mainly due to low temperature in the primary zone. This may also be a contributing factor to the significant NH_3 slip observed for this case, as shown in Fig. 2(d).

Furthermore, wall heat loss may also influence the emission characteristics of the staged NH_3 flames investigated in the present study. Since the combustor was intentionally uninsulated to provide optical access for flame diagnostics, heat losses through the quartz confinement and secondary air injection section may reduce the local flame temperature, particularly near the wall and in the secondary zone. Lower temperatures can suppress NH_3 oxidation and reduce OH radical concentrations, leading to incomplete NH_3 conversion and increased NH_3 slip. The reduced temperatures inhibit temperature-sensitive N_2O decomposition reactions, which may contribute to the increased N_2O emissions observed for the AS-OI-L100 configuration. Similar effects of wall heat loss on NH_3 combustion emissions have been reported previously in NH_3 swirling flames interacting with combustor walls and in studies investigating heat-loss effects in reacting systems [45]. This opens the scope of future work that can focus on quantifying heat-loss effects using insulated combustor configurations and conjugate heat-transfer analysis.

For a given $\phi_{overall}$, the emission trends observed for different AS configurations are strongly influenced by the secondary air mixing and penetration characteristics. Since the secondary air was injected near the wall, the injection orientation and staging location governed the jet penetration depth and interaction with the primary rich flame. OI can promote stronger radial penetration and more uniform mixing, whereas TI may generate enhanced swirl and near-wall recirculation. Furthermore, changes in $\phi_{overall}$ altered the secondary air jet momentum and consequently the local mixing intensity. Therefore, the observed variations in NO, NH_3, and N_2O emissions are closely linked to the mixing behavior of the secondary air injection.

These observations highlight the strong interplay between injection mode, staging location, and $\phi_{overall}$ for the control of the emissions. OI promotes better mixing and local O_2 availability, through the high secondary air impinging velocity enhancing NO oxidation while minimising NH_3 slip. Larger staging distances, such as 200 mm, provide improved interaction between primary and secondary air streams, leading to more uniform temperature and species distribution and consequently better NO mitigation.

Overall, among the AS configurations tested, AS-OI-L200 demonstrates the most favorable performance under lean conditions ($\phi_{overall}$ = 0.85–0.91), achieving 73–77 % NO reduction with minimal NH_3 slip (<5 ppm). This underscores the importance of selecting an appropriate combination of injection mode and staging location to optimise emission reduction while maintaining low NH_3 slip based on the equivalence ratio.

3.2. Effect of combined plasma and air staging on emissions

In this section, the flame morphology and emission profile of the combined plasma and AS have been analysed. It can be seen from Fig. 3 that, for the no-plasma cases, the flame shapes remain largely similar between OI and TI, indicating that the orientation of secondary air alone does not drastically alter the overall flame structure. However, introducing secondary air at the 100 mm location significantly shortens the flame, which can be attributed to an increased local burning rate caused by enhanced mixing of secondary air with the fuel-rich region.

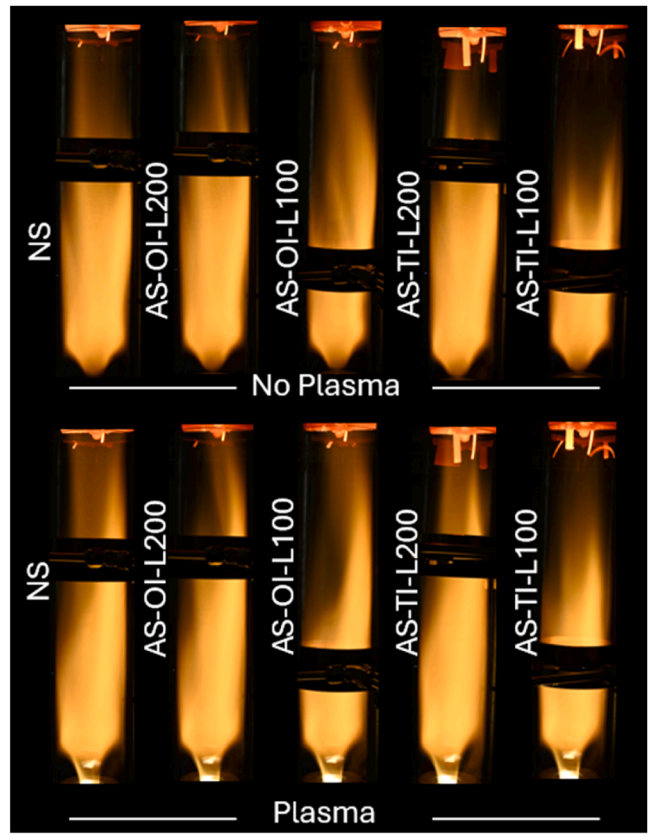

Fig. 3. Direct photography of NH_3-air flames for different AS configurations at $\phi_{overall}$=0.9.

This effect is more pronounced in AS-TI-L100 and AS-OI-L100 compared to their L200 counterparts, where the flame length remains relatively extended due to later injections and longer residence time for fuel-air interactions.

The actuation of plasma, in contrast, produces a significant change in flame morphology. Plasma generates strong rotating filamentary discharges, which create local ignition points and enhance turbulence and

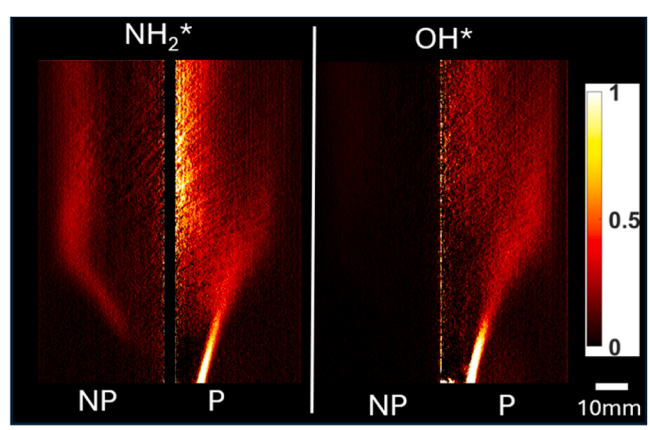

Fig. 4. Abel-deconvoluted chemiluminescence images of NH_2* and OH* for TS-OI-L200 case. (NP: No-plasma, P: With plasma).

NH_2* and OH* radical formation as shown in Fig. 4. This results in a more stabilised flame with brighter visual appearance. The plasma-induced changes dominate over the differences caused by injection orientation or position, highlighting the critical role of plasma in controlling flame stabilisation and radical distribution.

Fig. 5 shows the combined effects of plasma and air staging on the emission profiles of NO, NO_2, N_2O, and NH_3 for different AS configurations. For the NS cases, NO emissions follow similar trend as that of without plasma with $\phi_{overall}$. A reduction of approximately 36–38 % in NO is observed at $\phi_{overall} = 0.85$ and 0.9 compared to no-plasma cases, primarily due to the formation of plasma-induced NH_2 radicals and limited OH production. This is attributed to preferential fuel-side plasma activation by electron-impact dissociation of NH_3 ($NH_3 + e = NH_2 + H + e$), while limited plasma–air interaction suppresses OH-generating pathways, unlike in conventional fully premixed plasma-assisted combustors [31,33].

Furthermore, as compared to no-plasma case, N_2O emissions remain below 29 ppm in most cases as shown in Fig. 5, although AS-OI-L100 shows a marked increase to approximately 90 ppm at $\phi_{overall} = 1.0$ (Fig. 2), likely due to reduced local combustion temperatures, which limit N_2O decomposition. Overall, the AS-OI-L200 configuration provides the best compromise between effective NO mitigation and low NH_3 slip.

Fig. 6(a) and Fig. 6(b) illustrate the effect of plasma on the NO and NH_3 emission for different AS configurations at $\phi_{overall}$ =0.85 and 0.9 respectively. It is evident from Fig. 6 that the NH_3 and NO trends are

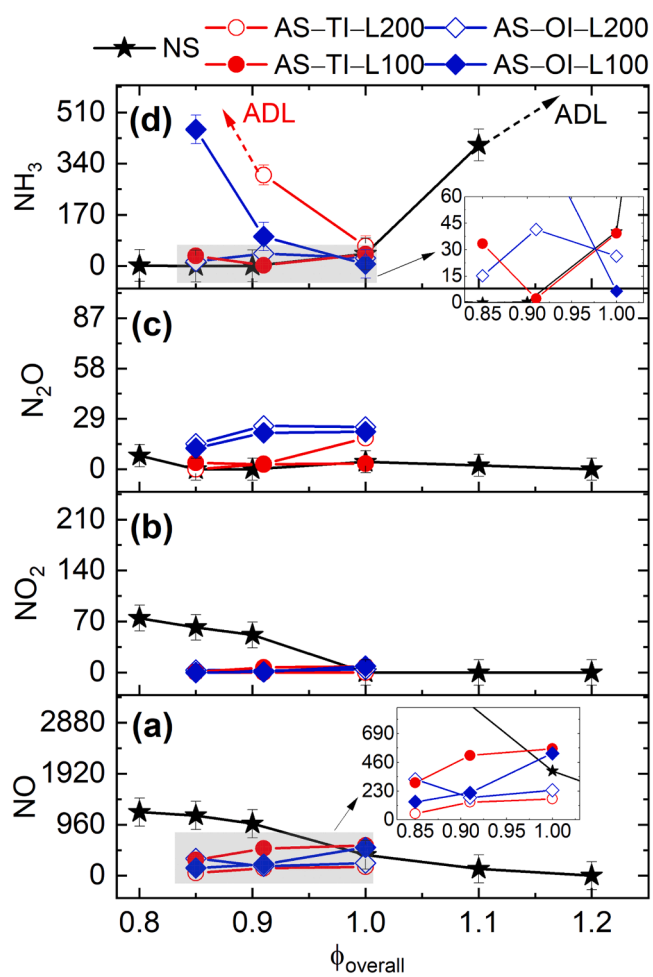

Fig. 5. Variation of (a) NO, (b) NO_2, (c) N_2O and (d) NH_3 with $\phi_{overall}$ for combined plasma and AS cases at fixed ϕ_{pri} =1.1 (All emissions are normalized to dry 15 % O_2). ADL: Above detection level.

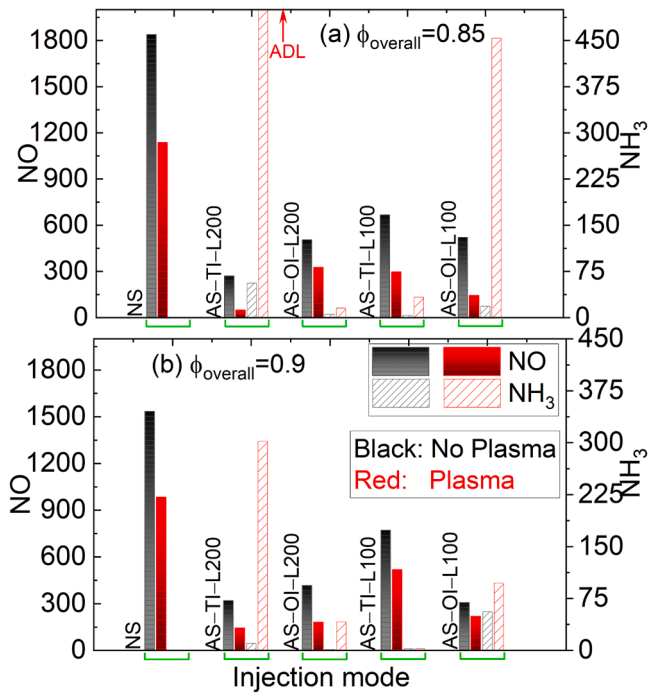

Fig. 6. Effect of plasma on the NO and NH_3 emission for different AS configurations at (a) $\phi_{overall}$ =0.85 and (b) $\phi_{overall}$ =0.9.

strongly influenced by the injection orientation and position. The TI generates strong swirl and promotes rapid local mixing of secondary air with the fuel-rich zone, which enhances NO reduction but can lead to higher NH_3 slip due to incomplete NH_3 oxidation. The OI, in contrast, produces milder swirl and more uniform mixing, allowing effective NO reduction while minimising NH_3 slip.

Similarly, the injection position affects residence time and radical interactions. This means that earlier injection (L100) introduces secondary air close to the fuel inlet, promoting early mixing but sometimes causing higher NH_3 slip under lean conditions due to insufficient combustion time. In contrast, later injection (L200) increases the combustion timescale in the primary stage, enabling more complete plasma-assisted combustion, thereby reducing NO_x emissions and minimizing NH_3 slip during the staging process. As a result, configurations such AS-TI-L200 and AS-OI-L100 exhibit the highest NO reductions (78–96 %) at lean $\phi_{overall}$, but these benefits come at the cost of excessive NH_3 slip, which increases further under leaner conditions. In comparison, AS-OI-L200 achieves a balanced performance, attaining a 71 % NO reduction with only 15 ppm NH_3 slip at $\phi_{overall} = 0.85$ (Fig. 6(a)), and up to 82 % NO reduction with 41 ppm NH_3 slip at $\phi_{overall} = 0.9$ (Fig. 6(b)). AS-TI-L100 performs similarly, achieving a 74 % NO reduction with 33 ppm NH_3 slip at $\phi_{overall} = 0.85$, while showing a more moderate 47 % NO reduction at higher $\phi_{overall}$ with negligible NH_3 slip.

3.3. Reaction sensitivity analysis

In this section, a detailed sensitivity analysis is conducted to identify the dominant reactions governing NO production and consumption under plasma-assisted and no-plasma conditions. The sensitivity of top ten important reactions participating in the NO_x production-consumption pathways are considered in the present sensitivity analysis (Fig. 7). For plasma-assisted premixed NH_3-air combustion, the primary plasma-induced reactions involve vibrationally excited N, O, and N_2 species. These species are generally formed through plasma interaction with air. These reactions mainly occur within the plasma reactor, while their direct influence on NO chemistry in the downstream combustion zone is relatively limited due to the short interaction time

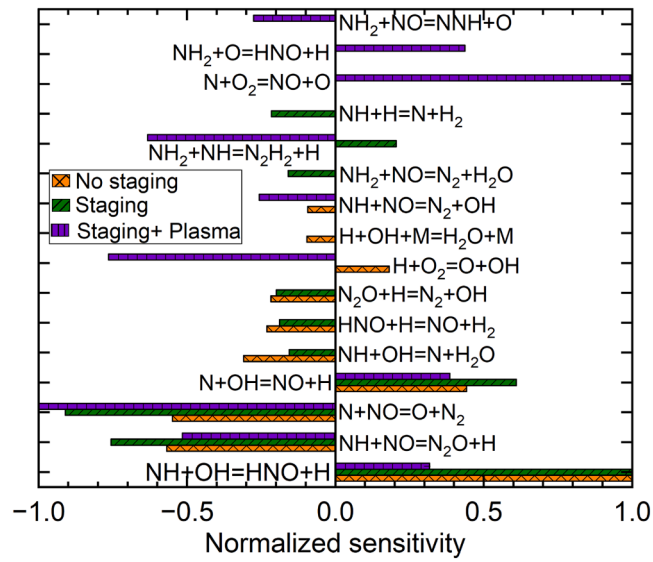

Fig. 7. Sensitivity analysis of NO in primary flame zone. orange: NS, no plasma, green: secondary air =10SLPM, no plasma, purple: secondary air=10SLPM, with plasma.

and rapid radical conversion [46]. However, in the present study, the plasma discharge is mainly confined to the NH_3 stream, resulting in limited plasma–air interaction. Consequently, the contribution of vibrationally excited N, O, and N_2 species to NO chemistry in the combustion zone is relatively small compared to more stable intermediate species such as NH_2 and HNO. Consequently, they do not appear among the ten most influential sensitivity reactions affecting NO in the combustion region. The key NH_3 ionisation reactions and NH_2 formation/consumption pathways are shown in Fig. S3 of the supplementary material, including reactions involving vibrationally excited species.

In an NH_3 combustion system at an equivalence ratio of 1.1, NO formation exhibits a strong dependence on both the local chemical environment and operational conditions. Under conventional combustion without plasma assistance, the primary NO formation pathway follows the Fuel-N mechanism, i.e., $NH_3 \rightarrow NH_2 \rightarrow NH \rightarrow HNO \rightarrow NO$. HNO serves as a critical intermediate for NO production, and its formation and consumption are regulated by competing reactions. It can be seen in Fig. 7 that, $NH + OH = HNO + H$ is positively sensitive, promoting NO formation, whereas $NH + NO = N_2O + H$ is negatively sensitive, partially suppressing NO accumulation by converting NH_x species into N_2O, which subsequently forms N_2. Under these conditions, NO peaks are typically observed within the mid-temperature range (approximately 1300–1500 K), and overall NO emissions are governed by the competition between production and reductive pathways [47] .

The introduction of plasma significantly alters the NO formation chemistry. Plasma-generated active radicals, notably N and O, enhance both NH_3 oxidation and NO generation. In particular, the reaction $N + O_2 = NO + O$ becomes the most positively sensitive, directly accelerating NO formation, whereas $N + NO = N_2 + O$ exhibits negative sensitivity by consuming O radicals, thereby indirectly limiting NO accumulation. While $NH + OH = HNO + H$ dominates positive sensitivity under no-plasma conditions, the positive sensitivity of $N + O_2 = NO + O$ is markedly enhanced with plasma, emphasising the decisive role of radical-mediated reactions in controlling NO production as shown in Fig. 7. Overall PAAC involves a trade-off between the conventional Fuel-N pathway and the plasma-induced N-radical oxidation pathway, driven by the enhanced radical pool that participates in both NO formation and NO consumption reactions. The results suggest that a controlled plasma–air interaction strategy, as employed in the present study, is essential to limit the excessive activation of NO-forming pathways while simultaneously suppressing the Fuel-N route through reduced HNO.

Air staging introduces an additional layer of complexity, modifying both local O_2 availability and NO formation dynamics. In the absence of plasma, air staging reduces local O_2 concentrations in fuel-rich zones, which decreases the flux of $N + O_2 = NO + O$ without significantly altering the relative sensitivities of other NO-related reactions such as $NH + OH = HNO + H$ and $NH + NO = N_2O + H$. This leads to an overall reduction in NO emissions compared to uniform air injections, demonstrating the influence of O_2 stratification on intermediate radical chemistry.

When plasma assistance is combined with air staging, NO emissions are further suppressed. Sensitivity analysis reveals that the negatively sensitive reaction $N + NO = O + N_2$ becomes dominant, while other NO consumption pathways are also enhanced. The plasma-generated radicals (N, O, H) accelerate both NH_3 oxidation and NO reduction, effectively shifting the dynamic balance toward net NO depletion. These results suggest that the combined effect of air staging and plasma assistance reduces NO emissions primarily by strengthening the $N + NO = O + N_2$ pathway, which represents the major NO sink in the system. Overall, the interplay between radical production, oxygen availability, and competing formation/consumption reactions provides a mechanistic explanation for the observed NO reduction under plasma-assisted, staged combustion conditions.

For future work, a more comprehensive parametric study covering a wider range of staging ratios, ϕ_{pri} and fuel staging is needed to further clarify the coupled effects of oxygen stratification and plasma-generated radicals on NO_x–NH_3 chemistry. In addition, extending the analysis to detailed spatial kinetics and transient behavior would help better resolve the local reaction pathways governing NO formation and depletion.

4. Conclusion

This study investigated the effects of air staging and combined plasma–air staging on NH_3–air combustion at a fixed at $\phi_{pri} = 1.1$. The influence of injection orientation and staging position on flame morphology and emissions was systematically analysed. The conclusions of this study are summarised below.

(1) Air staging significantly reduced NO emissions under lean conditions with AS-OI-L200 showing 73–77 % reduction and minimal NH_3 slip (<5 ppm). AS-TI-L200 achieved higher NO reduction (up to 85 %) but caused greater NH_3 slip, while L100 cases showed weaker mixing and lower effectiveness.
(2) Plasma activation enhanced radical generation and flame stability, offering an additional 36–38 % NO reduction. Combined plasma–AS cases, notably AS-OI-L200 and AS-TI-L200, achieved up to 96 % NO reduction though some lean tangential cases showed increased NH_3 slip.
(3) Overall, AS-OI-L200 provided the most balanced performance, demonstrating that optimized air injection orientation and staging position are key to achieving efficient, low-emission NH_3 combustion.
(4) Numerical analysis indicates that NO formation is strongly governed by radical chemistry and O_2 availability. Under conventional combustion, NO mainly follows the Fuel-N pathway, with $NH + NO = HNO + H$ as the dominant positive reaction. Plasma activation increases N and O radicals, shifting the mechanism toward N-activated oxidation where $N + O_2 = NO + O$ becomes dominant. When combined with air staging, reduced local O_2 and enhanced NO consumption via $N + NO = O + N_2$ lead to a net reduction in NO emissions, explaining the synergistic emission control observed experimentally.

CRediT authorship contribution statement

B Aravind: Writing – original draft, Methodology, Investigation, Funding acquisition, Formal analysis, Data curation, Conceptualization. **Ziyu Wang:** Writing – review & editing, Methodology, Investigation, Formal analysis, Data curation. **Syed Mashruk:** Writing – review & editing, Resources. **Agustin Valera-Medina:** Writing – review & editing, Supervision, Resources, Funding acquisition.

Declaration of competing interest

The authors declare that they have no known competing financial interests or personal relationships that could have appeared to influence the work reported in this paper.

Acknowledgements

This work was supported by the European Union Project CAIPIRI-NH3A, under the GA Number 101191768. Views and opinions expressed are, however, those of the author(s) only and do not necessarily reflect those of the European Union or CINEA. Neither the European Union nor the granting authority can be held responsible for them. The research was undertaken at Cardiff University's Thermofluids Lab (W/0.17) with invaluable technical support from Mr. Jonathan Martin. Information on the data underpinning this publication, including access details, can be found in the Cardiff University Research Data Repository at https://doi.org/10.17035/cardiff.30126730.10.17035/cardiff.34069809.

Supplementary materials

Supplementary material associated with this article can be found, in the online version, at doi:10.1016/j.proci.2026.106657.

References

[1] A. Valera-Medina, H. Xiao, M. Owen-Jones, W.I. David, P.J. Bowen, Ammonia for power, Prog Energy Combust Sci 69 (2018) 63–102.
[2] S. Mashruk, H. Shi, L. Mazzotta, C.E. Ustun, B. Aravind, R. Meloni, A. Alnasif, E. Boulet, R. Jankowski, C. Yu, Perspectives on NO X emissions and impacts from Ammonia combustion processes, Energy & Fuels 38 (2024) 19253–19292.
[3] H. Kobayashi, A. Hayakawa, K.K.A. Somarathne, E.C. Okafor, Science and technology of ammonia combustion, Proc. Combust. Inst. 37 (2019) 109–133.
[4] M. Zhang, X. Wei, J. Wang, Z. Huang, H. Tan, The blow-off and transient characteristics of co-firing ammonia/methane fuels in a swirl combustor, Proc. Combust. Inst. 38 (2021) 5181–5190.
[5] A.A. Khateeb, T.F. Guiberti, G. Wang, W.R. Boyette, M. Younes, A. Jamal, W. L. Roberts, Stability limits and NO emissions of premixed swirl ammonia-air flames enriched with hydrogen or methane at elevated pressures, Int J Hydrogen Energy 46 (2021) 11969–11981.
[6] A.A. Khateeb, T.F. Guiberti, X. Zhu, M. Younes, A. Jamal, W.L. Roberts, Stability limits and NO emissions of technically-premixed ammonia-hydrogen-nitrogen-air swirl flames, Int J Hydrogen Energy 45 (2020) 22008–22018.
[7] O. Kurata, N. Iki, T. Matsunuma, T. Inoue, T. Tsujimura, H. Furutani, H. Kobayashi, A. Hayakawa, Performances and emission characteristics of NH3–air and NH3CH4–air combustion gas-turbine power generations, Proc. Combust. Inst. 36 (2017) 3351–3359.
[8] S. Mashruk, E.C. Okafor, M. Kovaleva, A. Alnasif, D. Pugh, A. Hayakawa, A. Valera-Medina, Evolution of N2O production at lean combustion condition in NH3/H2/air premixed swirling flames, Combust Flame 244 (2022) 112299.
[9] C.D. Ávila, S. Cardona, M. Abdullah, M. Younes, A. Jamal, T.F. Guiberti, W. L. Roberts, Experimental assessment of the performance of a commercial micro gas turbine fueled by ammonia-methane blends, Applications in Energy and Combustion Science 13 (2023) 100104.
[10] K. Ryu, G.E. Zacharakis-Jutz, S.-C. Kong, Effects of gaseous ammonia direct injection on performance characteristics of a spark-ignition engine, Appl Energy 116 (2014) 206–215.
[11] Y. Tu, H. Zhang, T.F. Guiberti, C.D.A. Jimenez, H. Liu, W.L. Roberts, Experimental and numerical study of combustion and emission characteristics of NH3/CH4/air premixed swirling flames with air-staging in a model combustor, Appl Energy 367 (2024) 123370.
[12] K.D.K.A. Somarathne, E.C. Okafor, A. Hayakawa, T. Kudo, O. Kurata, N. Iki, H. Kobayashi, Emission characteristics of turbulent non-premixed ammonia/air and methane/air swirl flames through a rich-lean combustor under various wall thermal boundary conditions at high pressure, Combust Flame 210 (2019) 247–261.
[13] S. Li, L. Zhang, X. Li, P. Fu, H. Zhou, Numerical analysis of NH3-CH4-air mixing quality effects on NO x formation in an air-staged gas turbine model combustor, Frontiers in Energy (2025) 1–14.
[14] C. Liu, H. Yang, X. Li, C. Ruan, L. Yu, X. Lu, Attenuation of thermoacoustic instabilities in a swirl-stabilized NH3–CH4–air combustor with secondary air injection, Exp Fluids 65 (2024) 88.
[15] E.C. Okafor, K.K.A. Somarathne, R. Ratthanan, A. Hayakawa, T. Kudo, O. Kurata, N. Iki, T. Tsujimura, H. Furutani, H. Kobayashi, Control of NOx and other emissions in micro gas turbine combustors fuelled with mixtures of methane and ammonia, Combust Flame 211 (2020) 406–416.
[16] D. Pugh, P. Bowen, A. Valera-Medina, A. Giles, J. Runyon, R. Marsh, Influence of steam addition and elevated ambient conditions on NOx reduction in a staged premixed swirling NH3/H2 flame, Proc. Combust. Inst. 37 (2019) 5401–5409.
[17] D. Pugh, A. Valera-Medina, P. Bowen, A. Giles, B. Goktepe, J. Runyon, S. Morris, S. Hewlett, R. Marsh, Emissions performance of staged premixed and diffusion combustor concepts for an NH3/air flame with and without reactant humidification, J Eng Gas Turbine Power 143 (2021) 051012.
[18] C.D.A. Jimenez, A. Macfarlane, M. Younes, A. Jamal, M. Dunn, T.F. Guiberti, A. R. Masri, W.L. Roberts, Effects of secondary air injection on the emissions and stability of two-stage NH3-CH4-air swirl flames, Proc. Combust. Inst. 40 (2024) 105723.
[19] C.D.A. Jimenez, A. Macfarlane, F. Campuzano, S. Cardona, M. Dunn, T.F. Guiberti, A.R. Masri, W.L. Roberts, Fuel blend and secondary air injection effects on the stability, morphology, and dynamics of two-stage NH3-CH4/H2 swirl flames, Proc. Combust. Inst. 41 (2025) 105817.
[20] S. Mashruk, H. Xiao, A. Valera-Medina, Rich-Quench-lean model comparison for the clean use of humidified ammonia/hydrogen combustion systems, Int J Hydrogen Energy 46 (2021) 4472–4484.
[21] D.V. de Campos, T.F. Guiberti, E.-t. Es-sebbar, D.A. Lacoste, Effects of reactants stratification and pre-heating on the stabilization and emissions of partially cracked ammonia swirl flames, Proc. Combust. Inst. 40 (2024) 105231.
[22] Z.A. Shah, G. Mehdi, P.M. Congedo, D. Mazzeo, M.G. De Giorgi, A review of recent studies and emerging trends in plasma-assisted combustion of ammonia as an effective hydrogen carrier, Int J Hydrogen Energy 51 (2024) 354–374.
[23] A.M. Radwan, M.C. Paul, Plasma assisted NH3 combustion and NOx reduction technologies: principles, challenges and prospective, Int J Hydrogen Energy 52 (2024) 819–833.
[24] Y. Ju, W. Sun, Plasma assisted combustion: progress, challenges, and opportunities, Combust Flame 162 (2015) 529–532.
[25] D.A. Lacoste, Flames with plasmas, Proc. Combust. Inst. 39 (2023) 5405–5428.
[26] J. Choe, W. Sun, T. Ombrello, C. Carter, Plasma assisted ammonia combustion: simultaneous NOx reduction and flame enhancement, Combust Flame 228 (2021) 430–432.
[27] G.T. Kim, J. Park, S.H. Chung, C.S. Yoo, Effects of non-thermal plasma on turbulent premixed flames of ammonia/air in a swirl combustor, Fuel 323 (2022) 124227.
[28] Z. Wang, B. Aravind, S. Mashruk, A. Valera-Medina, Experimental investigation on the effects of gliding arc plasma on the combustion characteristics of air stratified NH3 flames, Energy 336 (2025) 138413.
[29] Z. Wang, B. Aravind, S. Mashruk, A. Valera-Medina, Numerical investigation on the combustion characteristics of premixed NH3-air flames using gliding arc plasma, Journal of the Energy Institute 123 (2025) 102314.
[30] B. Aravind, Z. Wang, S. Mashruk, D.A. Lacoste, A. Valera-Medina, Novel strategy for combustion enhancement of NH3-air mixture using gliding arc plasma, Proc. Combust. Inst. 41 (2025) 105848.
[31] R. Ju, J. Wang, M. Zhang, H. Mu, G. Zhang, J. Yu, Z. Huang, Stability and emission characteristics of ammonia/air premixed swirling flames with rotating gliding arc discharge plasma, Energy 277 (2023) 127649.
[32] Q. Lin, Y. Jiang, C. Liu, L. Chen, W. Zhang, J. Ding, J. Li, Controllable NO emission and high flame performance of ammonia combustion assisted by non-equilibrium plasma, Fuel 319 (2022) 123818.
[33] Y. Tang, D. Xie, B. Shi, N. Wang, S. Li, Flammability enhancement of swirling ammonia/air combustion using AC powered gliding arc discharges, Fuel 313 (2022) 122674.
[34] J. Sun, Q. Huang, Y. Tang, S. Li, Stabilization and emission characteristics of gliding arc-assisted NH3/CH4/air premixed flames in a swirl combustor, Energy & Fuels 36 (2022) 8520–8527.
[35] S. Wang, X. Wei, M. Gu, Q. Lin, G. Luo, F. Hu, Flame characteristics and NO emission law of sliding arc plasma-assisted ammonia combustion, Combust Flame 274 (2025) 114000.
[36] X. Mao, H. Zhong, N. Liu, Z. Wang, Y. Ju, Ignition enhancement and NOx formation of NH3/air mixtures by non-equilibrium plasma discharge, Combust Flame 259 (2024) 113140.
[37] H. Zhong, X. Mao, N. Liu, Z. Wang, T. Ombrello, Y. Ju, Understanding non-equilibrium N2O/NOx chemistry in plasma-assisted low-temperature NH3 oxidation, Combust Flame 256 (2023) 112948.
[38] T.S. Taneja, P.N. Johnson, S. Yang, Nanosecond pulsed plasma assisted combustion of ammonia-air mixtures: effects on ignition delays and NOx emission, Combust Flame 245 (2022) 112327.
[39] M. Shahsavari, A.A. Konnov, A. Valera-Medina, M. Jangi, On nanosecond plasma-assisted ammonia combustion: effects of pulse and mixture properties, Combust Flame 245 (2022) 112368.
[40] H. Tang, S. Gubbi, W. Sun, Investigation of flame structure in plasma-assisted ammonia swirling flames using NH planar laser-induced fluorescence, Combust Flame 274 (2025) 114006.
[41] A. Gaydon, The Spectroscopy of Flames, springer science & business media, 2012.

[42] L.W. Crispim, P.H. Hallak, M.S. Benilov, M.Y. Ballester, Modelling spark-plug discharge in dry air, Combust Flame 198 (2018) 81–88.
[43] G. Dong, Y. Zhou, P. Ming, Z. Wu, H. Chen, Y. Huang, L. Li, Kinetics-based analysis of the gliding arc plasma assisted ammonia decomposition process towards vehicle on-board applications, Chemical Engineering Journal 505 (2025) 159443.
[44] J.A. Alnasif, J. Papp, M. Szanthoffer, A.G. Kovaleva, M. Turanyi, T. Valera Medina, A. Nagy, T, Compact kinetic model for the combustion of NH3/H2 mixtures, submitted to Journal of Ammonia Energy - (2025).
[45] E.C. Okafor, M. Tsukamoto, A. Hayakawa, K.K.A. Somarathne, T. Kudo, T. Tsujimura, H. Kobayashi, Influence of wall heat loss on the emission characteristics of premixed ammonia-air swirling flames interacting with the combustor wall, Proc. Combust. Inst. 38 (2021) 5139–5146.
[46] J. Liang, J. Tao, X. Huang, M. Gu, X. Meng, Y. Chao, S. Fang, K. Xiang, Mechanism of the synergistic enhancement of ammonia combustion and NO formation by the energy of a gliding arc plasma, Combust Flame 287 (2026) 114942.
[47] A.M. Elbaz, S. Wang, T.F. Guiberti, W.L. Roberts, Review on the recent advances on ammonia combustion from the fundamentals to the applications, Fuel Communications 10 (2022) 100053.